Journal of Applied Physics

RESEARCH ARTICLE | APRIL 24 2024

Hole and positron interaction with vacancies and p-type dopants in epitaxially grown silicon

Special Collection: Native Defects, Impurities and the Electronic Structure of Compound Semiconductors: A Tribute to Dr. Wladyslaw Walukiewicz

Fabio Isa ; Javier A. Schmidt ; Stefano Aghion ; Enrico Napolitani ; Giovanni Isella ; Rafael Ferragut

J. Appl. Phys. 135, 165704 (2024)
https://doi.org/10.1063/5.0179101

27 August 2024 14:29:37

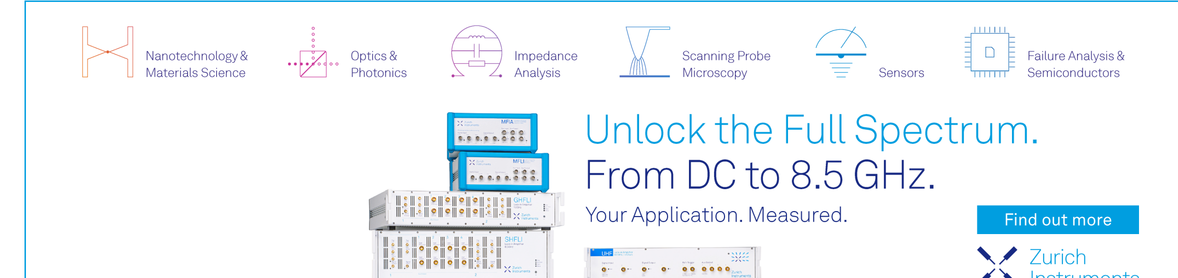

Journal of Applied Physics

ARTICLE

pubs.aip.org/aip/jap

Hole and positron interaction with vacancies and p-type dopants in epitaxially grown silicon

Cite as: J. Appl. Phys. **135**, 165704 (2024); doi: 10.1063/5.0179101
Submitted: 29 September 2023 · Accepted: 8 April 2024 ·
Published Online: 24 April 2024

View Online

Export Citation

CrossMark

Fabio Isa,[1,2] Javier A. Schmidt,[3] Stefano Aghion,[2,4] Enrico Napolitani,[5] Giovanni Isella,[2] and Rafael Ferragut[2,a)]

AFFILIATIONS

[1]Coherent, Binzstrasse 17, Zürich CH-8045, Switzerland
[2]L-NESS and Department of Physics, Politecnico di Milano, Via Anzani 42, Como I-22100, Italy
[3]Instituto de Física del Litoral y Facultad de Ingeniería Química, CONICET y Universidad Nacional del Litoral, Güemes 3450, Santa Fe S3000GLN, Argentina
[4]STMicroelectronics, Via Camillo Olivetti 2, Agrate Brianza I-20864, Italy
[5]Dipartimento di Fisica e Astronomia, Università di Padova and CNR-IMM, Via Marzolo 8, Padova I-35131, Italy

Note: This paper is part of the Special Topic on Native Defects, Impurities and the Electronic Structure of Compound Semiconductors: A Tribute to Dr. Wladyslaw Walukiewicz.

[a)]**Author to whom correspondence should be addressed**: rafael.ferragut@polimi.it

27 August 2024 14:29:37

ABSTRACT

The concentration of vacancies and impurities in semiconductors plays a crucial role in determining their electrical, optical, and thermal properties. This study aims to clarify the nature of the interaction between positrons and ionized *p*-type impurities, emphasizing the similarities they share with the interaction between holes and this type of impurity. An overall strategy for investigating defects in semiconductor crystals that exhibit a combination of vacancies and *p*-type impurities is presented. By using positron annihilation spectroscopy, in particular, Doppler broadening of the annihilation radiation, we quantify the concentration of vacancies in epitaxial Si crystals grown by low-energy plasma-enhanced chemical vapor deposition. The vacancy number densities that we find are $(1.2 \pm 1.0) \times 10^{17}\,\mathrm{cm}^{-3}$ and $(3.2 \pm 1.5) \times 10^{20}\,\mathrm{cm}^{-3}$ for growth rates of 0.27 and 4.9 nm/s, respectively. Subsequent extended annealing of the Si samples effectively reduces the vacancy density below the sensitivity threshold of the positron technique. Secondary ion mass spectrometry indicates that the boron doping remains unaffected during the annealing treatment intended for vacancy removal. This study provides valuable insights into the intricate interplay between vacancies and ionized impurities with positrons in semiconductor crystals. The obtained results contribute to advance the control and understanding of material properties in heterostructures by emphasizing the significance of managing vacancy and dopant concentrations.

© 2024 Author(s). All article content, except where otherwise noted, is licensed under a Creative Commons Attribution (CC BY) license (https://creativecommons.org/licenses/by/4.0/). https://doi.org/10.1063/5.0179101

I. INTRODUCTION

In the rapidly advancing technological paradigm of "More than Moore,"[1,2] the epitaxial integration of dissimilar materials is crucial to combine those with superior electrical, optical, and magnetic properties with cheap and reliable Si CMOS substrates. Unfortunately, due to different crystal lattice properties and out-of-equilibrium epitaxial growth conditions, extended and point defects, such as vacancies and interstitials, are introduced in the heterostructures. In particular, the electrical, optical, and thermal properties of semiconductors are significantly influenced by the concentration of vacancies and impurities as a function of the growth condition. In this regard, modeling and simulation prove to be invaluable tools for predicting the growth rates and structure morphology of epitaxial layers.[3,4] Given that doped layers are typically necessary for device fabrication, the coexistence of vacancies and ionized impurities is a common occurrence. Dopants play a critical role in determining the electrical conductivity of the semiconductor, while vacancies impact various material properties, including optical,[5,6] thermal,[7] mechanical,[8,9] and electrical ones.[10,11] Specifically, a high density of vacancies can also affect the carriers'

© Author(s) 2024

mobilities. Understanding and correlating the densities of vacancies and impurities in semiconductor crystals with epitaxial growth conditions is vital for tailoring specific material functionalities.

Positron annihilation spectroscopy (PAS) is a well-established method for investigating point defects in semiconductors and metals.[12,13] When a positron (e^+) is implanted into condensed matter, it annihilates with an electron emitting two 511 keV gamma-rays. The Doppler effect associated with the momentum of the annihilating electron–positron pair causes broadening in the energy spectrum of the annihilation gamma-rays. Positrons tend to localize in vacancy-type defects (neutral and negative) due to Coulomb repulsion from ion cores. By measuring the Doppler broadening (DB) spectra of the annihilation radiation, one can detect vacancy-type defects as the momentum distribution of electrons in defects differs from that in bulk materials. Ionized impurities also interact with positrons and influence the annihilation spectrum, particularly acceptor-type impurities. When p-type impurities are ionized, for instance, at room temperature, they carry a negative charge, serving as attractive centers for positrons.

These negative ions, however, do not offer an open volume for the positrons, and are, therefore, assumed to be shallow positron traps. At high temperatures, the thermal detrapping from the screened Coulomb potential becomes dominant and the influence of negative ions on positron trapping is reduced. However, the temperature at which thermal emission from negative ions overpasses trapping strongly depends on the dopant concentration, since the effect of ions has been observed up to temperatures of 300 K in electron-irradiated silicon[14] and of 550 K for electron-irradiated GaAs.[15] Consequently, distinguishing the contributions of vacancies and impurities in PAS measurements could be an issue, particularly in *p*-type materials with high dopant concentrations, as will be discussed in this work.

In this study, we grow epitaxial Si crystals using the low-energy plasma-enhanced chemical vapor deposition (LEPECVD) method.[16] LEPECVD allows for the growth of epitaxial films within a wide range of growth rates spanning from 0.01 to 10 nm/s. This technique utilizes a low-energy (∼10 eV) DC argon plasma to activate silane gas precursor molecules for Si deposition. The incorporation of other gases enables the deposition of doped layers. This epitaxial technique has been successfully employed to realize high crystal quality SiGe/Si 3D heterostructures free from threading dislocations,[17,18] virtual substrates,[19] and integrated devices such as infrared photodetectors[20] and optical interconnects.[21]

PAS has been used in the past to study epitaxially grown silicon. Schultz *et al.* studied silicon epilayers grown by molecular-beam epitaxy (MBE), obtaining evidence of defects at the interface and on the epilayer.[22] Schut *et al.* compared samples deposited by MBE and by solid-phase epitaxy, measuring a higher concentration of open-volume defects in the latter material.[23] Szeles *et al.* used a method of sequential etching to study the breakdown of epitaxy in samples deposited by MBE at low temperatures.[24] Rammukainen *et al.* observed the formation of a large concentration of vacancy clusters, coordinated with dopant atoms, in highly Sb-doped Si grown by MBE.[25] However, when samples present a combination of vacancy-like defects and dopant impurities, the contribution of both defects to the decrease in the positron diffusion length has not been clarified.

Using a combination of PAS measurements—interpreted according to the trapping model—[26–28] and secondary ion mass spectrometry (SIMS) determinations, we present a strategy to separate the contribution of vacancies and impurities to the e^+ diffusion length. Prolonged post-growth annealing treatments are used to reduce the vacancy concentration below the sensitivity threshold of the PAS technique, allowing for the isolated investigation of the effects of ionized impurities. In this context, similarities emerge between the interactions of positrons and holes with *p*-type impurities. By employing this comprehensive approach, we aim to advance the understanding of defects in semiconductor crystals, elucidating the intricate interplay between vacancies, impurities, and positrons. We emphasize that a high vacancy concentration significantly affects both carrier and positron mobilities. The results contribute to the control and customization of material properties in epilayers, paving the way for further advancements in semiconductor technologies.

II. EXPERIMENTAL METHODS

In this section, we describe the epitaxial Si growth by LEPECVD, annealing procedure, PAS, and SIMS equipment.

A. Epitaxial growth and annealing of Si samples

The epitaxial Si layers are deposited by LEPECVD on intrinsic (phosphorous concentration $< 9 \times 10^{11}$ cm^{-3}) 4-in. Si(001) substrates. Before epitaxial growth, the Si substrates are cleaned by a standard RCA bath,[29] dipped in 5% diluted HF solution for 30 s to strip the oxide, and rinsed in de-ionized water for 180 s. After outgassing in the load-lock for 15 min at $\sim 5 \times 10^{-7}$ mbar, the substrates are loaded into the reactor at $\sim 3 \times 10^{-9}$ mbar, and heated up to the growth temperature $T_g = 750$ °C at a rate of 1 °C/s. High purity 5 N silane (SiH_4) was used as the source gas, while diborane (B_2H_6) was used for *p*-type doping. The Si growth rate (G_r) was tuned to 0.27 or 4.9 nm/s by regulating the flux of the SiH_4 precursor gas, and the density and current of the DC Ar plasma.[30] The growth parameters of different Si samples are reported in Table I.

27 August 2024 14:29:37

TABLE I. List of Si samples and respective growth and annealing parameters. t_{Si}, τ_{growth}, G_r, and τ_{ann} and T_{ann} indicate the epitaxial Si thickness, the duration of the deposition, the Si growth rate, and the post-growth annealing time and temperature, respectively. All Si samples are grown at a temperature of $T_g = 750$ °C. The B number density in the epitaxial Si samples is measured by SIMS as illustrated in Fig. 2. These values are the average and standard deviation calculated in the first 2.4 μm from the top surface.

Sample name	t_{Si} (μm)	τ_{growth} (s)	G_r (nm/s)	τ_{ann} (h)	T_{ann} (°C)	Average B number density (cm^{-3})
HR	5	1020	4.9	…	…	$(4.9 \pm 0.2) \times 10^{17}$
HRA	5	1020	4.9	10	650	$(4.9 \pm 0.3) \times 10^{17}$
LR	2.4	8890	0.27	…	…	$(1.12 \pm 0.04) \times 10^{18}$
LRA	2.4	8890	0.27	10	650	$(1.10 \pm 0.05) \times 10^{18}$

© Author(s) 2024

The Si samples deposited at $G_r = 4.9$ and 0.27 nm/s are labeled through the whole text as HR (high rate) and LR (low rate), respectively.

Both LR and HR Si samples were annealed (labeled LRA and HRA, respectively) *ex situ* for 10 h at a temperature $T_{ann} = 650\,°C$ and a pressure of 5×10^{-7} mbar, by means of halogen lamps in a dedicated vacuum chamber. The annealing temperature is chosen, according to Refs. 31 and 32, to activate the diffusion of vacancies avoiding boron migration. After the annealing, the samples were slowly cooled to room temperature at a rate of 0.6 °C/min.

B. Positron annihilation spectroscopy

Variable-energy positron annihilation spectroscopy was used for this study. The Doppler broadening (DB) spectra of the annihilation radiation were measured as a function of the incident positron implantation energy in the range from 0.1 to 18 keV. For each incident energy, spectra with more than 1×10^6 events under the annihilation peak were obtained. DB spectra were measured at the L-NESS Positron Laboratory (Como), using an electrostatic low-intensity positron beam and conventional high-resolution Ge detectors (FWHM of 1.32 keV at 511 keV). The spectra were characterized by the *S* parameter, defined as the ratio of the number of annihilation events over the energy range $|511\,\text{keV}-E| \leq 0.85$ keV (around the center of the annihilation peak) to the total number of counts in the complete annihilation peak ($|511\,\text{keV}-E| \leq 4.25$ keV). This parameter reflects the relative contribution of low-momentum electrons to the total annihilation probability.[11] Because of their low momenta (low degree of localization), mainly annihilation events with valence electrons contribute to the region of the *S* parameter. The *S* parameter is the fraction of positrons annihilating with low-momentum valence electrons and correlates with vacancy-type defects and their concentration.

The positrons' diffusion into a crystal after thermalization is considered, in many works, from a classical point of view. This is a collective description based on the hypothesis of a concentration gradient profile of the diffused particles (Fick's laws). A more realistic description considers individual particles, with positrons being implanted one at a time, as actually happens in positron annihilation spectroscopy experiments. The positron becomes a completely quantum object, a de Broglie wave function extended over the entire crystal lattice. For example, in a "perfect" crystal without defects, the wave function of a single positron is represented as a Bloch function, where the maximum probability density is found in the interstitial locations. If the crystal contains a defect, such as a vacancy, the wave function tends to localize in this open location, away from the positive atomic nuclei.

In *n*-type doped semiconductors, at room temperature, the dopant is ionized, promoting the extra electron to the conduction band. In this condition, the impurity becomes a positively charged center, and the positron wave function has a minimum at this site. On the other hand, *p*-type impurities under the same conditions promote holes to the valence band, leaving the acceptor as a negatively charged center. In this case, the positron wave function tends to localize at the location of the impurity.

In this work, we study a complex case, a silicon crystal that contains two attractive centers for the positron: "vacancy-like defects" and "p-type boron impurities." Vacancies with different charge states generally form in silicon, depending on the arrangement of the dangling bonds.[33] For instance, vacancies associated with dislocations tend to be neutral or negative.[34] A high concentration of ionized p-type dopants and neutral/negatively charged vacancies are competitive attractive centers for positrons. The positron wave function will tend to localize in both negative centers, depending on the nature of the different defects. Vacancies are known to provide deep positron traps, with more than 1 eV binding energy. The binding energy of the positron to a negative ion can be calculated from a simple model based on the effective mass,[35]

$$E_{ion} = \frac{13.6\ eV}{\epsilon^2}\frac{m^*}{m_0}\frac{Z^2}{n^2}, \tag{1}$$

where ε is the relative dielectric constant, m^* the effective mass of the positron, m_0 the mass of the electron, Z the charge of the negative ion, and n the principal quantum number. The relative dielectric constant of silicon is 11.7[36] and the effective mass of the positron is $m^* = 1.5\ m_0$ due to phonons and the shielding of the electron cloud.[37] For an ion of charge $Z = 1$, the state with $n = 1$ has a binding energy $E_{ion} = 0.149$ eV [Eq. (1)]. Therefore, even when negative ions are shallower traps than vacancies, they are alternative annihilation sites for positrons, as shown below. The principle of detailed balance leads to the following expression for the ratio between the emission rate from the state of the positron trapped by the ion, δ, and the trapping rate, κ,[38]

$$\frac{\delta}{\kappa} = \frac{1}{N_{ion}}\left(\frac{m^* k_B T}{2\pi\hbar^2}\right)^{3/2} e^{-E_{ion}/k_B T}. \tag{2}$$

For the binding energy of 0.149 eV found previously, a temperature of 298 K and a number density of ionized acceptors $N_{ion} = 1 \times 10^{18}\ \text{cm}^{-3}$, the ratio of Eq. (2) results $\frac{\delta}{\kappa} = 0.069$. Therefore, the emission rate is about 14 times lower than the capture rate, so the positron will have a high probability of annihilating once it has been captured. These conclusions do not change substantially even if we take the effective mass of the positrons $m^* = m_0$. A basic simulation using the above-mentioned parameters shows that about 50%–80% of the positrons are annihilated while bound to a negative ion. This means that, when the concentration of negatively charged impurities is greater than the concentration of vacancies, the probability of capture and annihilation of the positron while bound to these defects is competitive with the probability of annihilation in vacancies.

From the measurement of the *S* parameter as a function of the positron implantation depth performed in this work, it is possible to estimate the "classical" diffusion length of the positrons, which can be assimilated to the extent of the positron wave function within a smooth envelope function.[39] The concept of a slowly varying envelope function to describe the behavior of the positron wave function over the whole crystal has been developed within the so-called pseudopotential scheme, and then more comprehensively generalized, as discussed in the review of Puska and Nieminen.[40] If the implantation depth is less than this characteristic distance of

27 August 2024 14:29:37

© Author(s) 2024

the wave function, positrons tend to be emitted into the vacuum as a single particle or in the form of positronium (the positron–electron bound state).

The evolution with the implantation energy of the averaged positron S parameter was modeled by means of the VEPFIT program.[41] One of the outputs of this program is the positron mean diffusion length, L_{diff}, within the sample under study. This quantity represents the average distance that positrons travel before their annihilation, and it is proportional to the square root of the product of the positron diffusion coefficient D_{e+} and the positron average lifetime τ before annihilation ($L_{diff} = \sqrt{D_{e+}\,\tau}$). The diffusion length is shortened by the presence of defects and ionized impurities that act as trapping or scattering centers. In the framework of the positron trapping model, if a material is characterized by a uniform distribution of one kind of point defects, like vacancies, the defect concentration per host atom n is given by the relation,[42]

$$n = \frac{1}{\nu_d\ \tau_{ref}}\left[\left(\frac{L_{ref}}{L_{diff}}\right)^2 - 1\right], \tag{3}$$

where ν_d is the positron trapping coefficient associated with the kind of defects considered, τ_{ref} and L_{ref} are the positron lifetime and diffusion length in a reference crystal, and L_{diff} is the mean diffusion length in the material with defects. The reference crystal could be a defect-free material or, as analyzed in Sec. IV, a crystal with a background concentration of dopants (p-type).

C. Secondary ion mass spectrometry

SIMS measurements are employed to measure the B concentration profile in the Si samples before and after the annealing process. The measurements are performed with a CAMECA IMS-4f by sputtering an 8 keV O_2^+ beam over a $250 \times 250\,\mu m^2$ area, while collecting B^+ secondary ions from a central region, 60 μm in diameter, to avoid crater edge effects. Concentration scales are calibrated against a commercial certified standard with an accuracy of ±5%. Depth scales are calibrated by measuring the crater depths with a TENCOR P17 profilometer and assuming a constant erosion rate, with an overall accuracy of ±2%.

III. RESULTS

Positron annihilation spectroscopy was employed to study defects in micrometer-thick silicon films epitaxially grown by LEPECVD. The relative S_r parameter is plotted as a function of the positron implantation energy in Fig. 1. S_r is the ratio of the measured S parameter to that of bulk silicon ($S_r = S/S_{Si}$, where $S_{Si} \approx 0.539$). The mean implantation depth of the positron, calculated with the Makhov profile,[11] is shown in the upper abscissa as well. The S_r parameter at the sample's surface, where there are a few nanometers of native silicon dioxide, is lower than that of bulk silicon for all the samples ($S_r < 1$). As the implantation energy increases, S_r tends to a plateau value $S_r = 1$. As a rule of thumb, the higher the implantation energy at which the saturation value is reached, the greater the positron diffusion length, since more deeply implanted positrons will be able to reach the surface. For

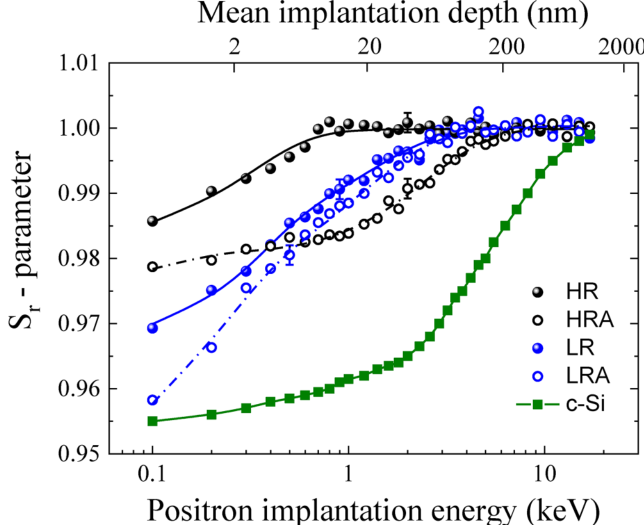

FIG. 1. S_r, the S parameter relative to the value in bulk silicon ($S_r = S/S_{Si}$), is presented as a function of the positron implantation energy for the crystalline silicon substrate (green squares) and for the epitaxial silicon grown at a low rate (blue symbols) and at a high rate (black symbols), before and after annealing. The continuous and dashed lines represent the best fits of the data points calculated with the VEPFIT software.[31] In the upper abscissa, the mean implantation depth values are also shown.

27 August 2024 14:29:37

example, in the case of the intrinsic and annealed Si sample, depicted with green squares in Fig. 1, the positron diffusion length is the longest and S_r tends to saturate at the highest implantation energy, above 10 keV in this case.

Looking at Fig. 1 and comparing the samples in the as-deposited state, it is clear that the high-rate sample (HR, black spheres) reaches the plateau value at a lower energy than the low-rate sample (LR, blue spheres). Therefore, the positron diffusion length for the HR sample should be lower than that of the LR sample. This is confirmed by the analysis with the VEPFIT software. The continuous and dashed lines in Fig. 1 represent the best fits obtained, and the main results are listed in Table II. For the analysis, we used a bilayer model composed of a first superficial layer of silicon dioxide and a second layer of silicon. It was not necessary to add an electric field to perform the fits. It has been found

TABLE II. Positron diffusion lengths in the low- and high-rate-grown Si samples before and after annealing obtained by VEPFIT (see the text). The model includes a naturally grown SiO_2 layer of 4 nm, whose positron diffusion length was set to 10 nm. The mean variance of the curve fits shown in Fig. 1 is 1.4.

Sample name	L_{diff} (nm)
LR	21 ± 3
LRA	26 ± 3
HR	2.0 ± 0.5
HRA	76 ± 4

© Author(s) 2024

TABLE III. Concentration of vacancies per silicon atom (*n*) and vacancy number density (*N*) for HR and LR samples, calculated from Eq. (3) and using the values reported in Table II.

Sample name	L_{diff} (nm)	L_{ref} (nm)	n	N (cm^{-3})
LR	21 ± 3	26 ± 3	$(2.5 \pm 2.0) \times 10^{-6}$	$(1.2 \pm 1.0) \times 10^{17}$
HR	2.0 ± 0.5	76 ± 4	$(6.5 \pm 3.0) \times 10^{-3}$	$(3.2 \pm 1.5) \times 10^{20}$

out that, before the annealing, the positron diffusion length for the HR sample is $L_{diff}^{HR} = (2.0 \pm 0.5)$ nm and for the LR sample it is $L_{diff}^{LR} = (21 \pm 3)$ nm. Compared with the intrinsic crystalline silicon substrate (grown by the Czochralski method, c-Si, filled green squares in Fig. 1), it is evident that the diffusion length of the positron in the crystal is much larger than that in the epitaxial layers, resulting in a diffusion length $L_{diff}^{c-Si} = 245$ nm. Therefore, the presence of defects in the epitaxial layers is clear, but their nature and concentration are still unclear.

As already mentioned in Sec. II B, the *S* parameter depends on the concentration of Si vacancies as well as on the concentration of acceptors impurities like B atoms. Therefore, the strategy to disentangle this complex problem has been to perform PAS and SIMS measurements before and after the thermal annealing treatment to separate the two different contributions that affect the positron diffusion length. The thermal treatment was chosen in order to nearly eliminate the presence of vacancies from the grown Si layers.[27,28] SIMS measurements were performed so as to evaluate the distribution of B atoms within the epitaxial Si layers and also to ensure that, as will be shown hereafter, the B distribution does not change due to the annealing.

From Fig. 1 it is clear that the annealing dramatically increased the positron diffusion length in the case of the high-rate-grown samples (HRA, black open circles), while the increase after annealing for the low-rate-grown samples is much less noticeable (LRA, blue open circles), as explained below. The result of the fit with the VEPFIT software (dashed lines in Fig. 1) is that the positron diffusion lengths increased to $L_{diff}^{HRA} = (76 \pm 4)$ nm for the HRA sample and $L_{diff}^{LRA} = (26 \pm 3)$ nm for the LRA sample. This experimental evidence can be considered as a hint of the higher concentration of vacancies that the LEPECVD introduces inside the thin films at high growth rates. Under the hypothesis that the thermal treatment successfully removes the vacancies without affecting the B concentration, as demonstrated below based on SIMS results, Eq. (3) has been applied to the *S* parameter results (LRA and HRA in Fig. 1). In this case, two separated cases were studied with two different B background concentrations. Equation (3) was then applied for each B concentration with and without vacancies. For both cases, the positron diffusion length of the reference material (L_{ref}) is the one evaluated after the annealing (LRA and HRA), the positron trapping coefficient associated with the vacancies in silicon is[43] $\nu_d \sim 10^{15}$ s^{-1}, and the positron mean lifetime in silicon is $\tau_{ref} \sim 225$ ps.[44] The vacancy concentrations obtained, along with the diffusion lengths used in Eq. (3), are shown in Table III. The vacancy number density for the silicon grown at a high rate, $[N]^{HR} = (3.2 \pm 1.5) \times 10^{20}$ cm^{-3}, is three orders of magnitude higher than the vacancy number density for the low-rate sample, $[N]^{LR} = (1.2 \pm 1.0) \times 10^{17}$ cm^{-3}. In Table III, *n* is the concentration of vacancies per Si atom and *N* is the number density, calculated multiplying the concentration by the number density of silicon atoms ($\approx 5 \times 10^{22}$ atoms/cm^3).

As previously stated, these PAS results stand under the hypotheses that the thermal treatment does not change the boron number density. This assumption is validated by SIMS measurements presented in Fig. 2, where the number density of B atoms within the epitaxial Si layers is measured as a function of depth. From these SIMS results, it is possible to draw the following conclusions.

First, the distribution of B atoms is constant through the whole investigated depth, both for the HR and LR samples. Indeed, by averaging the B number density in a depth of 2.4 μm from the top surface, we obtain $[B]^{HR} = (4.9 \pm 0.2) \times 10^{17}$ cm^{-3} and $[B]^{LR} = (1.12 \pm 0.04) \times 10^{18}$ cm^{-3} for the Si HR (black spheres) and Si LR (blue spheres) samples, respectively. This finding indicates that once the growth parameters are fixed, i.e., substrate temperature, chamber pressure, and Si growth rate, the B incorporation does not change significantly during the epitaxial deposition. In the case of the Si LR sample, the measurement has been prolonged to depths larger than 2.4 μm to characterize both the intrinsic Si (001) substrate and the layer/substrate interface. The latter appears sharp, whereas the former shows a number density level of about

27 August 2024 14:29:37

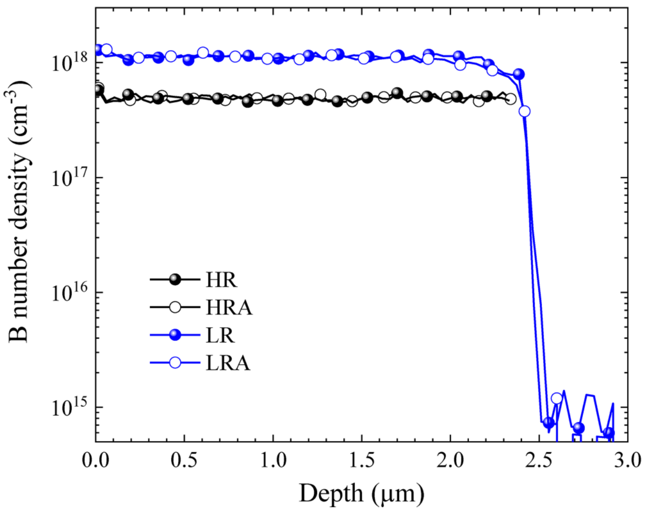

FIG. 2. B number density measured by SIMS as a function of depth from the top surface of the epitaxial layer. The SIMS measurements are performed on Si deposited at 4.9 and 0.27 nm/s before and after annealing, indicated as HR (black spheres), LR (blue spheres), HRA (black open circles), and LRA (blue open circles), respectively.

© Author(s) 2024

1×10^{15} cm^{-3}, which is compatible with a background induced by the measurement and should not be ascribed to a real B contamination present in the substrate. It is worth noting that such a measurement background level is orders of magnitude lower than the B number density measured in the grown layers, thus it does not affect the measurement accuracy.

Second, there is no evident effect of the prolonged annealing at 650 °C on the distribution of B impurities. Indeed, for both annealed Si HRA (black open circles) and LRA (blue open circles) samples, the measured average B number densities are $(4.9 \pm 0.3) \times 10^{17}$ and $(1.10 \pm 0.05) \times 10^{18}$ cm^{-3}, respectively. These values are equal within the error margin to those obtained before the annealing process.

The number density values of B measured by SIMS in the LR and HR samples (Fig. 2) are consistent, within the experimental error, with those derived from resistivity measurements conducted on the same samples using the four-point probe van der Pauw method. The resistivity measurements demonstrate the effective activation of the boron impurities.

IV. DISCUSSION

The system under study presents a combination of vacancies and ionized boron impurities, both affecting the diffusion of positrons. For the sample prepared at a high rate, in the as-prepared state, vacancies clearly have the largest influence. This is so because the vacancies number density is $[N]^{\mathrm{HR}} = 3.2 \times 10^{20}$ cm^{-3}, while the boron number density is almost three orders of magnitude lower, $[\mathrm{B}]^{\mathrm{HR}} = 4.9 \times 10^{17}$ cm^{-3}. It is useful to compare the positron diffusion length to the average distance between attractive centers. The distance between these centers is estimated through the inverse of the cube root of the defect number density. This distance gives an estimate of the average separation between defects, which coincides with the side of a simple cubic structure. This simple calculation of the average distance between vacancies, assuming a random distribution, gives a value $d_V^{HR} \cong 1.5$ nm, consistent with the obtained diffusion length for the positron $L_{diff}^{HR} = 2$ nm. On the other hand, for the sample deposited at a low rate, the number density of vacancies is lower than the boron number density, since we have $[N]^{\mathrm{LR}} = 1.2 \times 10^{17}$ cm^{-3} and $[\mathrm{B}]^{\mathrm{LR}} = 1.12 \times 10^{18}$ cm^{-3}. Therefore, the positron scattering with ionized impurities is expected to be the dominant mechanism for the positron diffusion, and the larger diffusion length of $L_{diff}^{LR} = 21$ nm is of the same order of magnitude and, therefore, consistent with the larger average distances between boron acceptors of $d_B^{LR} \cong 10$ nm.

After the thermal treatment, performed with great care to remove the vacancies without affecting the boron distribution, the situation changes: now the high-rate sample has a diffusion length $L_{diff}^{HRA} = 76$ nm, larger than that of the low-rate sample, $L_{diff}^{LRA} = 26$ nm. This is consistent with a lower boron number density for the HR sample, $[\mathrm{B}]^{\mathrm{HRA}} = 4.9 \times 10^{17}$ cm^{-3} compared to $[\mathrm{B}]^{\mathrm{LRA}} = 1.1 \times 10^{18}$ cm^{-3}. Therefore, after removing the vacancies, the lower boron number density of the HRA sample leads to a larger diffusion length. The strategy that we have followed to separate the contribution of vacancies and dopants to the positron diffusion length has been to perform a controlled annealing to remove the vacancies without affecting the dopant distribution.

The carrier mobility μ in a semiconductor having both dopants and defects depends on (i) the phonon contribution, μ_{ph}; (ii) the impurity contribution, μ_{im}, that depends on the number density of the p- or n-type impurity; and (iii) the defect contribution, μ_d. If the scattering mechanisms are independent, the inverse mobilities add giving

$$\frac{1}{\mu} = \frac{1}{\mu_{ph}} + \frac{1}{\mu_{im}} + \frac{1}{\mu_d}. \tag{4}$$

In the present case, the carrier mobility μ_d associated with defects depends on the vacancy concentration. After the annealing treatment at 650 °C performed in this work, it was possible to efficiently reduce the vacancy concentration and increase the mobility associated with the scattering mechanism with defects. Therefore, the term corresponding to the inverse of the defect mobility in Eq. (4) becomes negligible compared to the contribution of the impurity and the phonon terms, since the global mobility is mainly affected by the terms with lower mobilities.

Einstein's relation, $D = \mu\, k_B T/q$, gives a direct link between the carrier drift mobility μ and the diffusion coefficient D, where k_B is Boltzmann's constant, T the sample absolute temperature, and q the absolute value of the electron charge. In the following, we show that, in a p-type semiconductor, positron diffusion follows the same law as that of hole diffusion [Eq. (5)], with different coefficients. Indeed, the diffusion coefficient of holes depends on the scattering with phonons, vacancies, and ionized impurities [Eq. (4)]. At a fixed temperature, the dependence of the hole diffusion coefficient (D_{h+}) on the impurity number density (N) can be described by a phenomenological expression,[45]

$$D_{h+}(N) = D_{min} + \frac{D_{max} - D_{min}}{1 + (N/N_{ref})^{\alpha}}, \tag{5}$$

where D_{min} and D_{max} are the minimum and maximum values of the diffusion coefficient, N_{ref} is a reference impurity number density, and α is an exponent describing the transition between D_{min} and D_{max} (asymptotic values indicated in Fig. 3). D_{max} depends only on the carrier mobility associated to phonon scattering.

In a quantum mechanical vision, the wavefunction of a free positron extends like a Bloch function over the crystal, but in the presence of a negatively charged ionized impurity like B^-, the wavefunction localizes in the neighborhood of the impurity, where it eventually annihilates. In a classical vision, the positron moves with the thermal velocity, undergoing scattering by defects and perceives the Coulombic attraction of the negatively charged impurities. In any case, the positron diffusion coefficient D_{e+} is expected to decrease as the boron number density increases, where the carrier or the positron mobilities are limited by the ionized impurities. Bauer-Kugelmann *et al.*[46] have estimated the positron diffusion coefficient for defect-free silicon samples as a function of the dopant number density; these results are presented in Fig. 3 (filled blue circles). Two points (filled triangles) have been added that correspond to the experimental results obtained in the present work: D_{e+} values for the HRA and LRA samples. In general, when the acceptor number density becomes higher than $\sim 4 \times 10^{19}$ cm^{-3}, the diffusion coefficient is no longer

27 August 2024 14:29:37

© Author(s) 2024

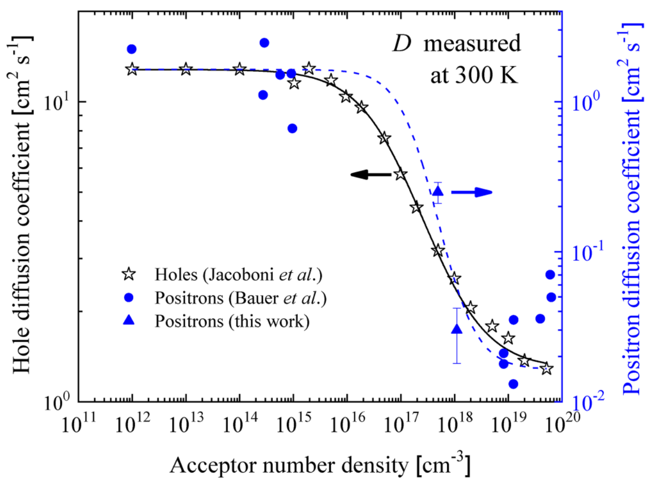

FIG. 3. Hole and positron diffusion coefficients as a function of boron number density. The hole diffusion coefficient is reproduced from Ref. 45 (black open stars). The positron diffusion coefficient is presented with blue symbols, filled triangles for the values estimated in this work, and filled circles for the values from Ref. 46. The lines correspond to fits with Eq. (5).

reliable due to the structural instability that may cause the formation of vacancy clusters and deep centers. The diffusion coefficients were calculated from $D_{e+} = L_{diff}^2/\tau$, where τ is the mean lifetime of positrons inside silicon (≈225 ps) and L_{diff} is the positron mean diffusion length in HRA and LRA samples (Table II).

Figure 3 also presents results obtained by Irvin[47] for the hole diffusion coefficient in crystalline silicon (open black stars), at room temperature and low electric field, as a function of the impurity number density. The solid line is a fit performed using Eq. (5), and clearly shows that, after a certain threshold number density, D_{h+} decreases with the increase of the dopant number density. Although the dispersion of the data points is much larger in the positron case, a similar dependence can be observed for D_{e+}, and a fit with Eq. (5) is also presented in Fig. 3 (dashed line, the last two points, for an acceptor number density $> 4 \times 10^{19}\,cm^{-3}$, were excluded from the fit). The D_{min} and D_{max} values of Eq. (5) are 1.7×10^{-2} and $1.65\,cm^2\,s^{-1}$ for positrons and 1.28 and $12.8\,cm^2\,s^{-1}$ for holes, respectively. As can be seen, D_{e+} changes by two orders of magnitude in the positron case, while D_{h+} only changes by one order of magnitude in the hole case. From the fit with Eq. (5), the values of N_{ref} and α for holes are $6 \times 10^{16}\,cm^{-3}$ and 0.79, respectively, in agreement with Ref. 45. Instead, for positrons, N_{ref} and α are estimated as $2 \times 10^{17}\,cm^{-3}$ and 1.3, respectively. Following the results presented in Fig. 3, we can conclude that, in a *p*-type silicon, the diffusion coefficient of positrons and holes follows a similar functional dependence. In fact, the fit represents the transition observed by Bauer-Kugelmann *et al.*[46] and the results of the present work. The transition zone for positrons is not well documented and contains only the experimental data added in the present work. This issue should be studied in more detail in future works.

Note that the transition zone is not observed by means of PAS in the case of *n*-type silicon at room temperature. Since the ionized donors are positively charged, positrons do not annihilate in their surroundings, and, therefore, the positron diffusion coefficient is not affected by the presence of donors at room temperature. This topic is discussed in Ref. 46, where D_{e+} is shown to be quite independent of the donor number density.

Since the diffusion of positrons and holes depends on the same scattering mechanisms, we can analyze an extreme and notorious case for positrons where the diffusion depends only on the contribution of phonons. This is the case for well-annealed intrinsic Si (or grown with a very low defect concentration), where the positron diffusion length—or the radius of action of the wavefunction—is about 250 nm (green symbols in Fig. 1). In this case, the thermalized positrons are mainly influenced by the interaction with phonons, and the equilibrium vacancy concentration at ambient temperature (300 K) is not detectable by PAS. Only when the vacancy concentration per Si atom reaches or exceeds the order of 10^{-8}–10^{-7}, it begins to give a signal compatible with positron trapping. This fact gives us a clear indication that when the concentration of vacancies in Si is greater than 10^{-7}, it begins to affect the mobility of the charge carriers. Therefore, epitaxial growth of Si with a vacancy concentration above this limit tends to reduce the device performance and structural stability. This information is crucial to realize semiconductor devices using epitaxial growth techniques. After growth, controlled annealing is necessary to ensure a low vacancy concentration.

V. CONCLUSIONS

In conclusion, we have used positron annihilation spectroscopy to study epitaxially grown silicon samples having a combination of vacancies and B impurities. The Doppler broadening, measured as a function of the positron implantation energy, in principle, gives spectra difficult to interpret due to the mixed effect of vacancies and impurities. Through a meticulous thermal treatment, we successfully reduced the vacancy concentration below the detection limit of the technique. This approach enabled us to estimate the initial vacancy concentration, which exhibited a strong dependence on the silicon growth rate. Specifically, the vacancy number density increased from $(1.2 \pm 1.0) \times 10^{17}\,cm^{-3}$ for the sample grown at 0.27 nm/s to $(3.2 \pm 1.5) \times 10^{20}\,cm^{-3}$ for the sample grown at 4.9 nm/s. This trend is predictable, since a lower growth rate allows growth with lower entropy, giving a longer time for the added Si atoms to adopt energetically favorable positions in the lattice, thus reducing the point defect density. The possibility of quantifying vacancy concentration is a notable feature of the PAS technique. The concentration of acceptors influences the positron diffusion length, since negatively charged impurities ionized at room temperature effectively localize the positron wave function. At this level, positron diffusion resembles hole diffusion, where the positron diffusion coefficient exhibits a functional dependence on boron concentration similar to the well-established dependence observed for the hole diffusion coefficient. To summarize, our findings emphasize the significance of controlling the concentrations of vacancies and dopant impurities in epilayers to tailor their material properties.

27 August 2024 14:29:37

ACKNOWLEDGMENTS

We acknowledge the Sinergia project NOVIPIX CRSII2_147639 of the Swiss National Science Foundation, the

© Author(s) 2024

European project GREEN Silicon (No. 257750). J.A.S acknowledges financial support from the RAICES program "Prácticas de formación académica y profesional en el exterior para argentinos/as" of the Argentinean Government. We are grateful to Dr. H. von Känel, Dr. A. Marzegalli, Professor L. Miglio, and Professor B. Batlogg for fruitful discussions. L. Bacci and N. Argiolas (University of Padova) are acknowledged for technical assistance.

AUTHOR DECLARATIONS

Conflict of Interest

The authors have no conflicts to disclose.

Author Contributions

Fabio Isa: Conceptualization (equal); Investigation (equal); Writing – original draft (equal). **Javier A. Schmidt:** Formal analysis (equal); Methodology (equal); Writing – review & editing (equal). **Stefano Aghion:** Data curation (equal); Investigation (equal); Methodology (equal); Writing – review & editing (equal). **Enrico Napolitani:** Investigation (equal); Validation (equal); Writing – review & editing (equal). **Giovanni Isella:** Conceptualization (equal); Resources (equal); Supervision (equal); Validation (equal); Writing – review & editing (equal). **Rafael Ferragut:** Conceptualization (equal); Formal analysis (equal); Investigation (equal); Methodology (equal); Supervision (equal); Writing – review & editing (equal).

DATA AVAILABILITY

The data that support the findings of this study are available within the article or are available from the corresponding author upon reasonable request.

REFERENCES

[1]M. Lundstrom, Science **299**, 210 (2003).
[2]R. Chau, B. Doyle, S. Datta, J. Kavalieros, and K. Zhang, Nat. Mater. **6**, 810 (2007).
[3]D. Raciti, G. Calogero, D. Ricciarelli, R. Anzalone, G. Morale, D. Murabito, I. Deretzis, G. Fisicaro, and A. La Magna, Mater. Sci. Semicond. Proc. **167**, 107792 (2023).
[4]Y. Yoshida and G. Langouche, *Defects and Impurities in Silicon Materials: An Introduction to Atomic-Level Silicon Engineering*, Springer Series "Lecture Notes in Physics" Vol. 916 (Springer, Tokyo, 2015).
[5]J. Hyun Kim, P. Bagheri, R. Kirste, P. Reddy, R. Collazo, and Z. Sitar, Phys. Status Solidi A **220**, 2200390 (2023).
[6]T. Iwasaki, F. Ishibashi, Y. Miyamoto, Y. Doi, S. Kobayashi, T. Miyazaki, K. Tahara, K. D. Jahnke, L. J. Rogers, B. Naydenov, F. Jelezko, S. Yamasaki, S. Nagamachi, T. Inubushi, N. Mizuochi, and M. Hatano, Sci. Rep. **5**, 12882 (2015).
[7]Y. Lee and G. S. Hwang, "Strong thermal conductivity dependence on arsenic-vacancy complex formation in arsenic-doped silicon," J. Appl. Phys. **126**, 195104 (2019).
[8]C. S. Peng, Y. K. Li, Q. Huang, and J. M. Zhou, J. Cryst. Growth **227–228**, 740 (2001).
[9]F. Isa, A. Marzegalli, A. G. Taboada, C. V. Falub, G. Isella, F. Montalenti, H. von Känel, and L. Miglio, APL Mater. **1**, 052109 (2013).
[10]E. Kamiyama, K. Sueoka, and J. Vanhellemont, "Vacancies in Si and Ge," in *Silicon, Germanium, and Their Alloys Growth, Defects, Impurities, and Nanocrystals*, edited by G. Kissinger and S. Pizzinipp (CRC Press, London, 2014), pp. 119–158.
[11]A. Chroneos and H. Bracht, Appl. Phys. Rev. **1**, 011301 (2014).
[12]A. Dupasquier, in *Positron Spectroscopy of Solids*, edited by A. Dupasquier and A. P. Mills, Jr. (IOS, Amsterdam, 1995).
[13]R. Krause-Rehberg and H. S. Lepner, *Positron Annihilation in Semiconductors*, Springer Series in Solid-State Sciences Vol. 127 (Springer, Berlin, 1999).
[14]A. Polity, F. Börner, S. Huth, S. Eichler, and R. Krause-Rehberg, Phys. Rev. B **58**, 10363 (1998).
[15]A. Polity, F. Rudolf, C. Nagel, S. Eichler, and R. Krause-Rehberg, Phys. Rev. B **55**, 10467 (1997).
[16]C. Rosenblad, H. R. Deller, M. Döbeli, E. Müller, and H. von Känel, Thin Solid Films **318**, 11 (1998).
[17]C. V. Falub, H. von Känel, F. Isa, R. Bergamaschini, A. Marzegalli, D. Chrastina, G. Isella, E. Müller, P. Niedermann, and L. Miglio, Science **335**, 1330 (2012).
[18]F. Isa, F. Pezzoli, G. Isella, M. Meduňa, C. V. Falub, E. Müller, T. Kreiliger, A. G. Taboada, H. Von Känel, and L. Miglio, Semicond. Sci. Technol. **30**, 105001 (2015).
[19]C. Rosenblad, H. von Känel, M. Kummer, A. Dommann, and E. Müller, Appl. Phys. Lett. **76**, 427 (2000).
[20]J. Osmond, G. Isella, D. Chrastina, R. Kaufmann, M. Acciarri, and H. von Känel, Appl. Phys. Lett. **94**, 201106 (2009).
[21]P. Chaisakul, D. Marris-Morini, J. Frigerio, D. Chrastina, M.-S. Rouifed, S. Cecchi, P. Crozat, G. Isella, and L. Vivien, Nat. Photonics **8**, 482 (2014).
[22]P. J. Schultz, E. Tandberg, K. G. Lynn, B. Nielsen, T. E. Jackman, M. W. Denhoff, and G. C. Aers, Phys. Rev. Lett. **61**, 187 (1988).
[23]H. Schut, A. van Veen, G. F. A. van de Walle, and A. A. van Gorkum, J. Appl. Phys. **70**, 3003 (1991).
[24]C. Szeles, P. Asoka-Kumar, K. G. Lynn, H.-J. Gossmann, F. C. Unterwald, and T. Boone, Appl. Phys. Lett. **66**, 2855 (1995).
[25]M. Rummukainen, I. Makkonen, V. Ranki, M. J. Puska, K. Saarinen, and H.-J. L. Gossmann, Phys. Rev. Lett. **94**, 165501 (2005).
[26]W. Brandt, *Positronium Annihilation* (Academic Press, New York, 1967).
[27]M. Bertolaccini and A. Dupasquier, Phys. Rev. B **1**, 2896 (1970).
[28]F. Tuomisto and I. Makkonen, Rev. Mod. Phys. **85**, 1583 (2013).
[29]W. Kern and D. A. Puotinen, RCA Rev. **31**, 187 (1970).
[30]C. Rosenblad, H. R. Deller, A. Dommann, T. Meyer, P. Schroeter, and H. von Känel, J. Vac. Sci. Technol. A **16**, 2785 (1998).
[31]P. G. Coleman, J. Phys.: Conf. Ser. **265**, 012001 (2011).
[32]H. Bracht, H. H. Silvestri, I. D. Sharp, and E. E. Haller, Phys. Rev. B **75**, 035211 (2007).
[33]D. W. Watkins, in *Identification of Defects in Semiconductors*, edited by M. Stavola (Academic Press, San Diego, 1999), Chap. 1, Vol. 51A.
[34]M. M. de Araújo, J. F. Justo, and R. W. Nunes, Appl. Phys. Lett. **90**, 222106 (2007).
[35]N. W. Ashcroft and N. D. Mermin, *Solid State Physics* (Holt-Saunders, New York, 1976), p. 579.
[36]D. A. Neamen, *Semiconductor Physics and Devices: Basic Principles*, 4th ed. (McGraw-Hill, New York, 2012).
[37]B. Bergersen and E. Pajanne, Phys. Rev. **186**, 375 (1969).
[38]M. Manninen and R. M. Nieminen, Appl. Phys. A **26**, 93 (1981).
[39]M. J. Stott and P. Kubica, Phys. Rev. B **11**, 1 (1975).
[40]M. J. Puska and R. M. Nieminen, Rev. Mod. Phys. **66**, 841 (1994).
[41]A. van Veen, H. Schut, J. de Vries, R. A. Hakvoort, and M. R. Ijpma, AIP Conf. Proc. **218**, 171–198 (1991).
[42]R. Krause-Rehberg, V. Bondarenko, E. Thiele, R. Klemm, and N. Schell, Nucl. Instrum. Methods Phys. Res. B **240**, 719 (2005).
[43]M. J. Puska, C. Corbel, and R. M. Nieminen, Phys. Rev B **41**, 9980–9993 (1990).
[44]P. Asoka-Kumar, K. G. Lynn, and D. O. Welch, J. Appl. Phys. **76**, 4935 (1994).
[45]C. Jacoboni, C. Canali, G. Ottaviani, and A. Alberigi Quaranta, Solid State Electron. **20**, 77 (1977).
[46]W. Bauer-Kugelmann, J. A. Duffy, J. Störmer, G. Kögel, and W. Triftshäuser, Appl. Surf. Sci. **116**, 231–235 (1997).
[47]J. C. Irvin, Bell Syst. Tech. J. **41**, 387 (1962).

27 August 2024 14:29:37

© Author(s) 2024